AIAA JOURNAL
Vol. 43, No. 4, April 2005

Flow Control of a Sharp-Edged Airfoil

Sergio Miranda,* Pavlos P. Vlachos,† and Demetri P. Telionis‡
Virginia Polytechnic Institute and State University, Blacksburg, Virginia 24061
and
Matthew D. Zeiger§
Aeroprobe Corporation, Blacksburg, Virginia 24060

An experimental study of active control of fully separated flow over a symmetrical circular-arc airfoil at high angles of attack was performed. The experiments were carried out in a low-speed, open-circuit wind tunnel with the airfoil at angles of attack from 10 to 40 deg. Low-power input, unsteady excitation was applied to the leading or trailing edge. The actuation was provided by the periodic oscillation of a 4% chord flap placed on the suction side of the airfoil and facing the sharp edge. Pressure measurements over the airfoil show that flow control increased the normal force coefficient by up to 70%. The application of flow control on sharp-edged aircraft wings could lead to improved maneuverability, innovative flight control, and weight reduction.

Nomenclature

C_n	=	section normal force coefficient
C_p	=	pressure coefficient, $2(p - p_\infty)/pU_\infty^2$
$\lvert C_n \rvert$	=	normalized section normal force coefficient $\equiv C_n/C_{n0}$
c	=	airfoil chord length
$\lvert F \rvert$	=	reduced frequency $\equiv f_a/f_s$
f	=	frequency
L	=	lift
p	=	pressure
$\lvert Sr \rvert$	=	normalized Strouhal number $\equiv Sr/S_o$
U	=	velocity
$\boldsymbol{x}$	=	chordwise coordinate
α	=	angle of attack
θ	=	flap angle
ρ	=	density

Subscripts

a	=	actuator property
pres	=	airfoil pressure side
s	=	shedding property
stall	=	static stall condition
suc	=	airfoil suction side
0	=	base case, no control applied
∞	=	freestream property

Introduction

SHARP edges are a common feature on many fighter aircraft. For wings with sharp edges, separation cannot be avoided even at low angles of attack. At moderate to high angles of attack, the suction side of the wings is dominated by separated flow that comprises large and small vortices, with a wide spectrum of length scales and frequencies.

Presented as Paper 2001-0119 at the 39th Aerospace Sciences Meeting, Reno, NV, 8–11 January 2001; received 29 May 2003; revision received 29 August 2004; accepted for publication 7 October 2004.

*Graduate Research Assistant, Department of Engineering Science and Mechanics.
†Assistant Professor, Department of Mechanical Engineering.
‡Professor, Department of Engineering Science and Mechanics.
§Chief Scientist, Corporate Research Center, 1700 Kraft Drive.

Flow control is gaining acceptance as a new design element of new radical air platforms. For a wide range of angles of attack of wings with rounded leading edges, it has been shown that many methods of microactuation are quite effective,[1–4] delaying separation or causing the separated flow to reattach. The flow over sharp geometries, however, involves different flow characteristics and requires different flow control mechanisms, as will be discussed later.

Attached flow cannot be sustained over a sharp leading edge, even at low angles of attack. One recent effort to control flow separating over a sharp leading edge was made by Zhu et al.[5] These authors carried out experiments with a rounded airfoil placed backward in a wind tunnel so that its sharp edge was leading. Although their tests were limited to an angle of attack of 27 deg, their results clearly indicated that increases in lift could be achieved.

Our goal here is to control the separated flow over sharp-edged wings. We should emphasize again the difference between "separated flow control" and "flow separation control." Both imply the condition of detached flow, but in a different flow scale. Fiedler[6] makes a clear distinction between these two flowfields. Weak separation can be defined as that where the separation point location is variable or undefined. This is the case for most flowfields around rounded leading-edge wings, where the separation point depends on the surface contour and flight condition. The strong separation case is that where the separation point is fixed. This applies to flows over sharp edges and to almost all bluff bodies with sharp corners. The separation point is fixed at a sharp edge or corner. Strong separation can be found over bodies with curved surfaces, but with walls that deviate sharply and away from the direction of the oncoming stream. For weak separation cases, passive and active controls are possible and lead to elimination or delay of flow separation. This is separation control. It is the aim of this paper to show that active control is possible for strong separation.

For rounded leading-edge airfoils, we may have weak or strong separation depending on the angle of attack. Wu et al.[7,8] make a clear distinction between these two cases. For angles of attack a few degrees beyond α_{stall}, the flow is not fully separated, and control is aimed at overcoming separation. For angles of attack much larger than α_{stall}, the flow is fully separated, and it is not possible to induce reattachment. It is difficult to control separation. In the first case, we have weak separation and control aims at eliminating separation altogether. In the second case we have strong separation and control techniques aim at managing the separated flow. The management of separated flow can be achieved by the utilization of low-power actuators, effectively controlling the shear layer roll up over the wing. This research falls into the category of active control of strong separation, that is, control of separated flow. In the present case, actuation is applied by means of an oscillating microflap at either the leading or the trailing edge.

For fully separated flow, it has been shown[2,5,7] that the most effective control frequency is the frequency of vortex shedding. This frequency scales with the width of the wake and the inverse of the freestream velocity. This was proved for cases of strong separation, including airfoils at high angles of attack. The present authors examined the data of Seifert and Pack,[9,10] as well as the results presented by Roos and Kegelman[11–13] and found that even for the cases of wall-bounded separated flows where only one shear layer is released in the wake, that is, where one sense of vorticity is shed, again control is most effective at a frequency that scales with the width of the obstruction and the inverse of the freestream velocity. The way we estimated these parameters is discussed in the next paragraph.

Seifert and Pack[9,10] studied the flow over a wall-mounted hump and demonstrated that flow-control methods can manage separated flow, not just separation. The flow over the hump was always separated, and the separation location was minimally affected by the flow control mechanism. This was, therefore, strong separation. They reported a natural reduced frequency of about 1.0, but they nondimensionalized this quantity with the distance from separation to reattachment. If one employs the width of their separated region instead, then the value of 0.25 emerges, which appears to be very close to the universal vortex shedding Strouhal number, valid for flows over bluff bodies or backward-facing steps. The present authors also considered the results obtained by Roos and Kegelman[11–13] of flow over backward-facing steps and found that the natural frequency dominating these flows is again the vortex shedding frequency. In addition, the reduced frequency is around 0.22 if their frequency is nondimensionalized in terms of the height of their step. In all cases, the universal constant associated with the shedding frequency scales with the width of the separated region.[14]

Alternate vortex shedding requires the interaction of two free shear layers of opposite sign to form a strong pattern, characterized by a distinct spike in the frequency domain. If the separated region is constrained on one side by a wall, as is the case of the Pack and Seifert hump, the Roos and Kegelman backward-facing step, or just the region over a stalled airfoil, the initiation of vortex shedding is somewhat impaired. This is displayed in the frequency domain by a very broad hump instead of a well-defined spike. However, vortex shedding can be easily triggered by a small disturbance, and this is exactly the effect of microactivation.

The significance of the preceding observations is that the separated flow over wings at low or high Reynolds numbers is receptive to disturbance frequencies equal to the vortex shedding frequency and its harmonics, but not to the most amplified frequency of the free shear layer. The second is an order of magnitude higher than the first and, in practice, is very hard to actuate. This is very significant because it implies that this mechanism can be implemented to control the flow over full-scale aircraft.

The experimental data of Seifert and Pack[8,9] also provide strong evidence that flow control methods are applicable to flows at high Reynolds numbers, namely, the order of 4×10^7, and high subsonic Mach numbers ($M = 0.6$). Such methods could, therefore, be employed to control the flow over fighter aircraft wings.

In this paper, results are presented of efforts to control separated flow over a double circular-arc airfoil. The wings of many such modern aircraft have cross sections that are very close in shape to a double circular arc. The basic aerodynamic performance of such an airfoil was studied in the 1950s by Cahil et al.,[15] and, thus, provides a good basis for comparisons. The flow was controlled by a microflap placed either at the leading edge or trailing edge. Results were presented at the 2001 AIAA Aerospace Sciences Meeting. Since then, some of these experiments were repeated to gain more confidence in the experimental method and to confirm that the results are repeatable. The basic flow characteristics were also compared with those obtained by Cahil et al.[15] The performance of leading-edge flaps like those tested by Cahil et al.[15] were contrasted with the performance of an oscillating microflap.

Experimental Setup and Equipment

Experiments were conducted in the Virginia Polytechnic Institute and State University Engineering Science and Mechanics wind tunnel. This is an open-circuit, low-speed tunnel, having a 5/1 contraction ratio and a test section measuring 0.51×0.51 m and 1.27 m in length. An axial fan driven by a 5-hp dc motor generates freestream velocities in the range of 4–20 m/s, with spanwise variation smaller than 1.5% and a maximum freestream turbulence intensity of about 0.5%.

An airfoil model with sharp leading and trailing edges was constructed. This is a symmetrical, circular-arc, 8% chord thickness airfoil. The chord length is 0.2032 m (8 in.), which results in an airfoil maximum thickness of 0.0162 m (0.64 in.). The model spans 0.5080 m (20 in.), 2 mm less than the tunnel width. End plates were employed to reduce end effects.

A total of 61 pressure taps were installed on the airfoil, 30 on the suction side and 31 on the pressure side. A Pressure Systems, Inc., model ESP pressure scanner was attached to the wall of the wind tunnel and used to measure the pressure distribution over the airfoil. The Tygon tubing length was kept less than 30 cm, thus allowing a frequency response of about 50 Hz. The ESP pressure scanner utilized in the current research was a 32-channel model with ± 10 in. of water pressure range. The static accuracy of the ESP, including nonlinearity, hysteresis, and nonrepeatability effects, is 0.10% of the full scale at constant temperature after a full calibration. However, because the instruments were operated below 10% of their full scale, the error was estimated at about 2–3% of the absolute of the maximum pressure measured. The calibration of the ESP pressure scanner was performed by the application of generated pressures and reading the pressures with a precision pressure transducer. For the standard pressure we used the Edwards Barocel model 590D precision pressure transducer, which has a range of 0–100 torr and an accuracy of 0.05% of the pressure reading plus 0.001% of the full scale of the unit. For the multiplexed signal coming from the ESP, Aeroprobe's AP-2500 signal processor was utilized, providing accuracy of 0.10% full scale.

The data acquisition was performed by the use of an eight-channel, A/D board, CIO-DASO8-AOL by Measurement Computing, with 20-kHz, programmable gain and a two-channel 12-bit D/A converter. Proprietary software was utilized that controls all of the required parameters on the ESP for calibration and data acquisition. An Edwards-Datametrics Barocel precision pressure transducer measured the tunnel pitot-static pressure and returned the freestream velocity. It was also used for the ESP static calibration. To maintain the required accuracy and stability of the measurements, the ESP was calibrated every 20 min. As a result, the overall pressure measurement uncertainty was estimated to be on the order of ± 8.2 Pa.

The actuation system consisted of a flat plate of 4% airfoil chord that covered the entire model span as shown in Fig. 1. In Fig. 1, the span of the model is not drawn to proportion with the chord to save space. The thickness of the plate was 0.127 mm (0.0050 in.) and was made out of brass. The flat plate was attached at one of its ends to a 1.27-mm (0.05-in.)-diam stainless-steel rod that works as the hinge between the flap and the wing. The rod was longer than the model span to link with the actuating mechanism on one side of the tunnel.

The flap was placed on one of the edges of the airfoil model. In its closed position, the flap edge coincided with the airfoil edge. The

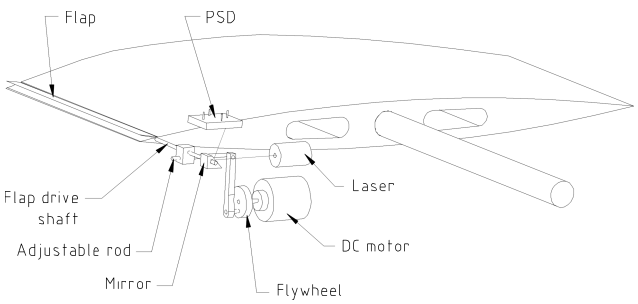

Fig. 1 Oscillating mechanism and laser positioning feedback mechanism.

surface of the airfoil was countersunk, so that in its parked position the flap did not protrude above the surface of the airfoil, nor did it extend over its edge. Because the airfoil model was symmetric, the flap could be placed on any side and edge for testing without the need to change parts or disassemble the model. In this work, the flap was always placed on the suction side of the airfoil, and the chord position was changed between the leading edge and trailing edge.

The flap was oscillated by a dc motor and an eccentric arrangement as shown schematically in Fig. 1. The motor shaft was connected to a flywheel equipped with an eccentric shaft. For the current research, the amplitude was fixed at 17 deg, set with an accuracy of ± 1 deg. The flywheel was balanced statically to work with minimum vibrations at frequencies in the order of 100 Hz.

An optical sensing system was employed to record and adjust the frequency of the flap oscillation. A position sensor detector (PSD) was used in conjunction with a laser pointer to give the exact position of the flap and its motion. The position sensing detector was a silicon photodiode that provides an output directly proportional to the position of a light spot on the detector active area. For this research, the On-Trak Photonics 2L10-2 Duo-Lateral two-dimensional PSD was utilized. The laser beam impinges on a small mirror attached on the flap driving rod. As shown in Fig. 1, the reflected beam then hits the PSD, which is positioned at an appropriate distance to allow the entire sensor photoelectric array to be used. With knowledge of the setup geometry, a precise flap location can be given at any time, and the flap oscillation frequency can be measured.

According to previous research, the most effective way of controlling the separated flow over the airfoil is by introducing disturbances with frequencies equal to the natural vortex shedding frequency and its harmonics. Wake measurements characterizing the vortex shedding were incorporated with a pitot rake of high-frequency-response pressure transducers. The pitot tubes measured the axial velocity variations in the wake of the airfoil, and the signals were recorded by the use of a RC Electronics ISC-16 board. The ISC-16 is a 16-channel, 12-bit, ± 10-V range board, capable of up to 1-MHz maximum sampling rate. Postprocessing of the signals to obtain the required frequencies was performed with a Welch periodgram. The rake includes six pitot tubes that spanned the wake width, connected to six high-frequency Endevco Model 8510B-2 piezoelectric pressure transducers with a 2-psig (13.79-Pa) full range. Signals from the six Endevco tranducers were amplified and conditioned by a Vishay Measurements Group, Inc., Instrument Division, signal conditioning amplifier Model 2210.

Two computers were employed for simultaneous data acquisition of airfoil pressure distribution and pressure rake measurements. The arrangement of instrumentation is shown schematically in Fig. 2. Both computers were triggered externally through a simple LOW–HIGH triggering signal coming from a function generator. To control, modify, and record the vortex shedding phenomena and adjust the actuator frequency, a two-channel Hewlett–Packard HP-3562A Dynamic Signal Analyzer was used as an experimental feedback tool. This reduces postprocessing time by aquiring real-time feedback of the physics of the experiment.

Experimental Results and Discussion

The flow was excited either at the leading edge or trailing edge. In both cases, the same flap mechanism was employed. The difference lies in the rotation of the airfoil by an angle of $(180 - 2\alpha)$ deg from the desired angle of attack α. The flap in both cases was located on the suction surface of the airfoil. If both vortex–vortex and sound–vortex resonance are present, this should be the best configuration, as suggested by Wu et al.[8]

This research is a parametric study of the effects of the flap actuation for different angles of attack and different actuation frequencies. The following procedure was adopted:

1) Set the desired angle of attack.
2) Set the freestream velocity.
3) By the use of the HP signal analyzer, check the natural shedding frequency.
4) Acquire data, no actuation applied.
5) Set excitation frequency.
6) Acquire data with actuation.

This implies an iterative process. The last two steps are repeated until data were recorded for all possible/desired excitation frequencies. Experiments were conducted for the parameter values listed in Table 1. No effort was made to correct for tunnel blockage. The purpose here was to compare the actuated flow with the base flow.

Base Flow Results

To understand the fundamentals of the fluid dynamics of the circular-arc airfoil at high angles of attack, results with no excitation were analyzed first. Pressure measurements taken over the surface of the airfoil were converted to pressure coefficients. The averaged values are displayed in Fig. 3 for different angles of attack. A sensor malfunction is found in the port placed at the 62.3% of

Table 1 Matrix of experimental parameters

Angle of attack, deg	Freestream velocity, m/s	Reynolds number, $[\times 10^5]$	Excitation configuration	Tunnel blockage, %
10	17.5	2.22	LE[a]	6.9
15	17.5	2.22	LE	10.9
20	17.5	2.22	LE/TE[b]	13.7
25	17	2.16	LE	16.9
30	17	2.16	LE/TE	20
40	15.5	1.97	LE/TE	25.7

[a]Leading edge. [b]Trailing edge.

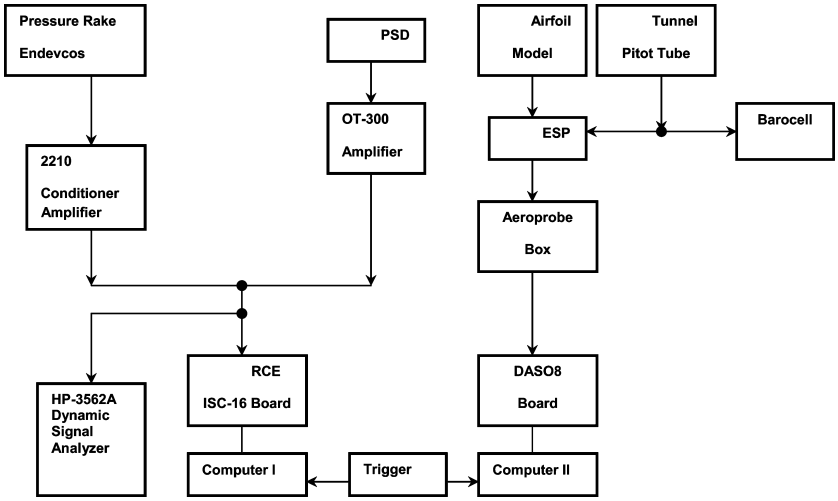

Fig. 2 Data acquisition system.

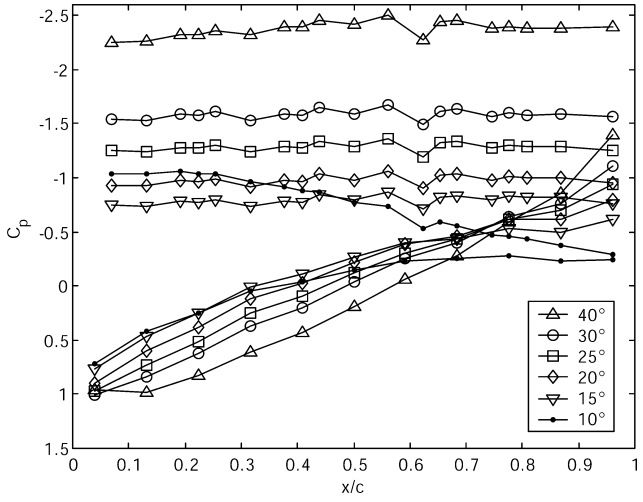

Fig. 3 Airfoil pressure coefficient distribution at different angles of attack, suction and pressure sides, no actuation; for Reynolds number, see Table 1.

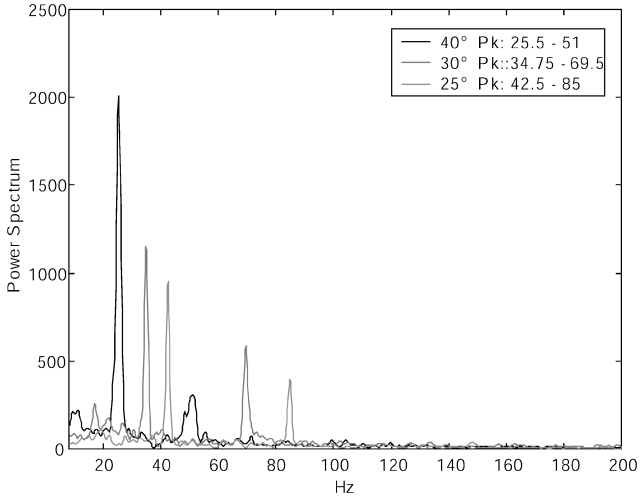

Fig. 4 PSD at angles 40–25 deg, pitot 3; Reynolds number and freestream velocity as in Table 1; Pk indicates peak values.

the chord on the suction side, but the error appears to be consistent. Figure 3 shows a flat average pressure distribution on the suction side for all angles of attack except $\alpha = 10$ deg. Flat pressure distributions are typical for fully separated flows. This finding confirms that, for the flow over a sharp-edged airfoil, separation is inevitable at the edges and reattachment is not possible, unless the airfoil is at very low angles of attack. For $\alpha = 10$ deg, we observe that over the first one-half of the wing the pressure is again uniform, but then in the aft one-half, there is a gradual drop of the curve. This drop represents an increase of pressure because here we plot the negative pressure coefficient. As the trailing edge is approached, the pressure coefficient of the two sides tends to a common value, signaling that the Kutta condition is satisfied in the average. The fore stagnation point is very near to the leading edge except for the highest angle of attack. This point moves toward the leading edge as incidence is decreased.

For the data presented herein, sensor 3 in the pitot rake, placed approximately in the middle of the wake, is chosen to monitor the flow. The effect of change of angles of attack on the vortex shedding characteristics as detected by this sensor is presented in Figs. 4 and 5. The vortical structure in the middle of the wake is characterized by two frequencies, a shedding frequency and its harmonic. This is true for the high angles, whereas the second component reduces in magnitude as the angle of attack diminishes. For the $\alpha = 20$ deg case, practically only one component is present.

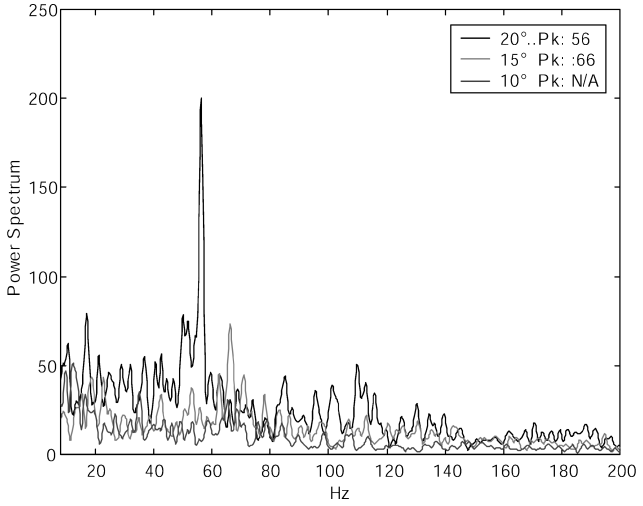

Fig. 5 PSD at angles 20–10 deg, pitot 3; Reynolds number and freestream velocity as in Table 1; Pk indicates peak values.

The $\alpha = 15$ deg case shows a broader peak on the PSD plot, which corresponds to a less organized flow. In the $\alpha = 10$ deg case, no peak is present. We believe this is because with one shear layer developing over the suction side and away from its companion shear layer, organized vortex shedding takes a little longer to develop and, thus, could not be detected close to the traling edge where the wake sensors are positioned. This could also imply that the flow is separated in the average, but a transient reattachment could exist. A recirculating bubble is probably formed, periodically bursting and shedding from the airfoil. The shedding process was later confirmed, and the corresponding data are included at the end of this paper. A Strouhal number is defined based on the frontal projection of the airfoil to the incident freestream:

$$Sr = (f_s c \sin\alpha)/U_\infty \tag{1}$$

This number was found to be between 0.2 and 0.22 for all angles of attack greater than 10 deg. Under the assumption of the same value of the Strouhal number for the case of $\alpha = 10$ deg, the shedding frequency for this angle of attack should be in the neighborhood of 100–110 Hz.

Control Cases

Data for different excitations were acquired by the application of disturbances at frequencies around the corresponding natural frequency of vortex shedding for each angle of attack and freestream velocity. All data were postprocessed and compared with the base case for each angle of attack. Because flow over a sharp-edged body maintains only a small dependence on the Reynolds number, the effects can be extrapolated to configurations of engineering importance.

Both the normal force coefficient $|C_n|$ and the Strouhal number $|Sr|$ were calculated at each excitation case and were normalized with respect to the base case. The normal force is estimated by integration of the pressure distribution, under the assumption that the wing is flat. This is a valid assumption due to the small thickness of the airfoil. A more accurate estimate would involve the multiplication of each element force pdx by the local value of the slope of the wing surface and integration over the chord. We estimated that neglecting the last factor introduces an error of less than 1–2%, which is well within the experimental error. Moreover, the enhancement of suction is stronger on the front rather than the aft part of the wing. Therefore, our estimates are conservative. For a flat plate, lift could be calculated simply by multiplying the normal force by the cosine of the angle of attack. For this reason, in this paper, we will use the term lift in place of reduced normal force. Frequencies are reduced with the natural shedding frequency for the case under consideration. Reduced normal force results are plotted

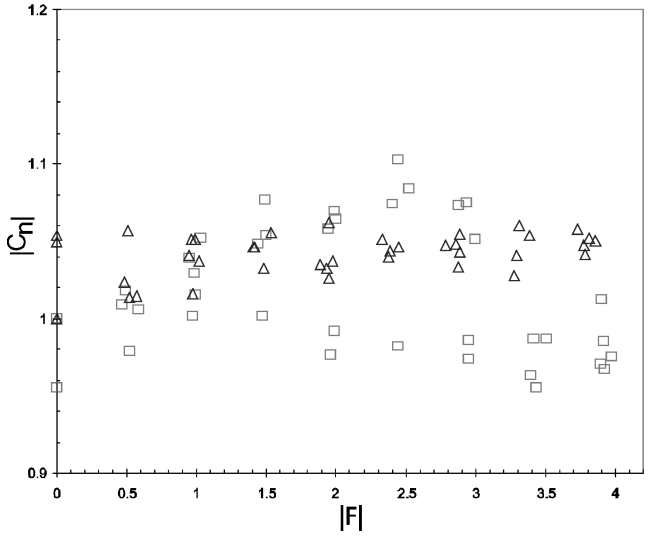

a) Normal force coefficient

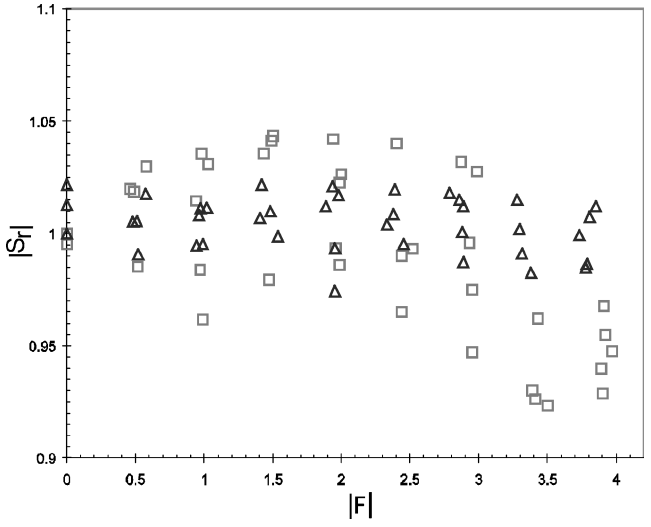

b) Strouhal number

Fig. 6 Variation with excitation frequency: angle of attack = 40 deg; □, leading-edge flap actuation and △, trailing-edge flap actuation.

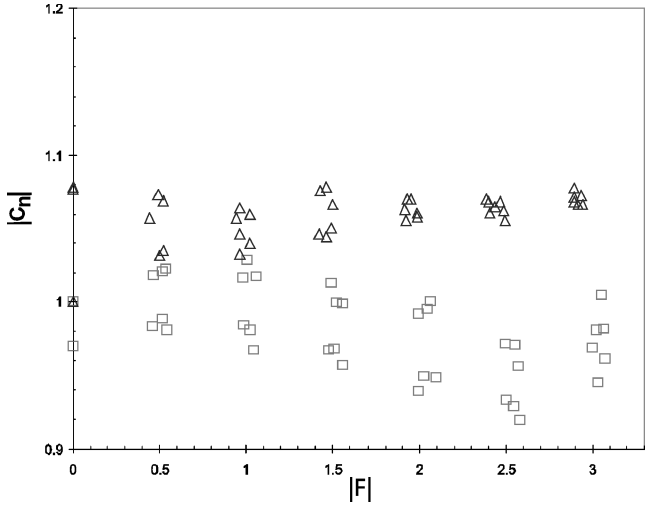

a) Normal force coefficient

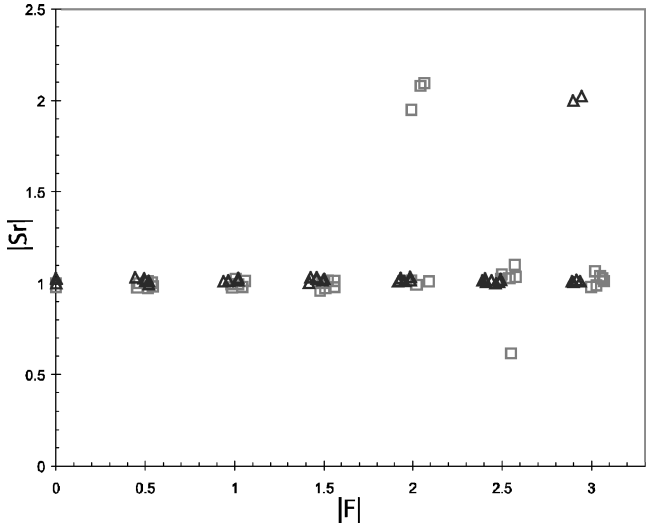

b) Strouhal number

Fig. 7 Variation with excitation frequency: angle of attack = 30 deg; □, leading-edge flap actuation and △, trailing-edge flap actuation.

against reduced frequency $|F|$ for each angle of attack and shown in Figs. 6–11.

The postprocessed data can be divided into two domains with respect to the actuation effectiveness. One is the high-angle-of-attack regime, namely, 25, 30, and 40 deg, and the other is the low-angle-of-attack regime, 20, 15, and 10 deg. Normal force increases in the higher-angle-of-attack regime are not as pronounced. Only a 10% increase is achieved in the best case for both the 40- and 25-deg angles, whereas in the 30-deg case, there is very little evidence of any effect on the normal force. This is quite disappointing, but was expected based on the predictions of Wu et al.,[7,8] who state that for optimal control the angle of attack cannot be too close to the stall angle, nor can it have large values. At the same time, note that the trailing-edge actuation results contradict the predictions of the same authors on the most effective placement of the excitation source, at least for the high-angles regime. Wu et al.[8] state that the leading-edge shear layer control should be the best actuation due to the upstream location and the high receptivity. This is probably true only for the angle-of-attack range that they refer to. In the current results, the trailing-edge flap gives for the $\alpha = 30$ deg case the only source of lift increment.

Both the 30- and 40-deg cases show a very interesting behavior. At first, the results appear to display large dispersions. When the experiment was repeated to confirm the repeatability of the results with an increase in the driving frequency by small increments to the highest value tested, followed by a decrease back to zero, a specific pattern emerged. Data points corresponding to increasing frequencies are above the mean, whereas points corresponding to decreasing values are below the mean. This is a clear hysteresis phenomenon.

Regime transition from the higher to the lower angles of attack seems to be in the neighborhood of 20–25 deg. In the high-frequency range, there is no frequency at which a clear improvement in lift can be realized. A net increase, although small, can be seen for the 25-deg case around the reduced frequency of 1. Normalized Strouhal number analysis shows no effective frequency changes due to actuation. For the angle of attack of 40 deg, no changes are observed. It is possible that at such angles of attack the microflap is well within the separated region and could not affect the free shear layer. This is definitely valid in the case of trailing-edge actuation.

Figure 7b shows shedding frequency shifting to the first harmonic or the subharmonic of the uncontrolled vortex shedding. The results in Fig. 8 are more affected by the excitation frequency. We observe that driving the flow with reduced frequencies up to 1.5 leaves the shedding frequency unaffected, that is, the reduced Strouhal number is 1. However, at about $F = 1.5$, the shedding frequency jumps and locks on to the subharmonic of the driving frequency. This is typical behavior of wake lock-on observed in flow-induced vibrations. Even more intriguing is that, although vortex shedding locks on the first harmonic of the natural frequency, the greatest increase in the normal force is observed if the flow is driven at the natural frequency.

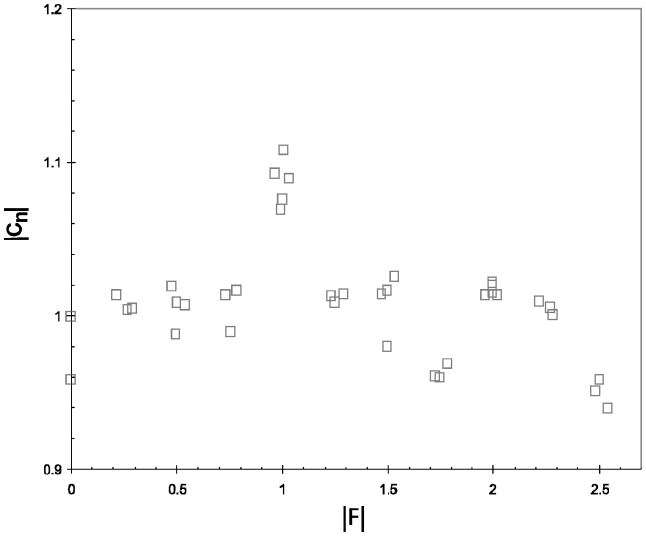

a) Normal force coefficient

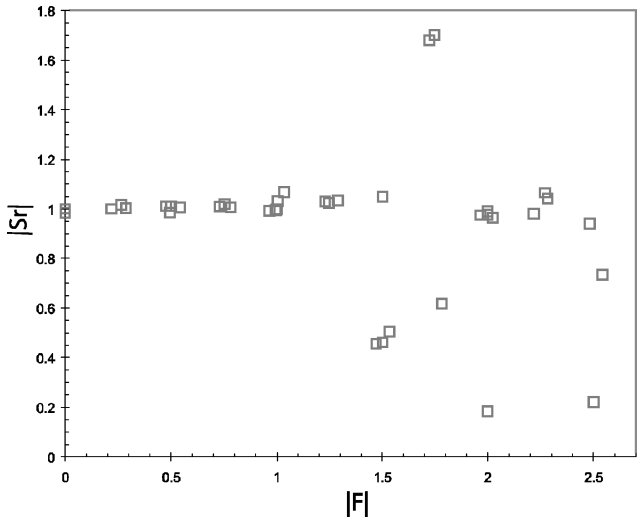

b) Strouhal number

Fig. 8 Variation with excitation frequency: angle of attack = 25 deg; □, leading-edge flap actuation.

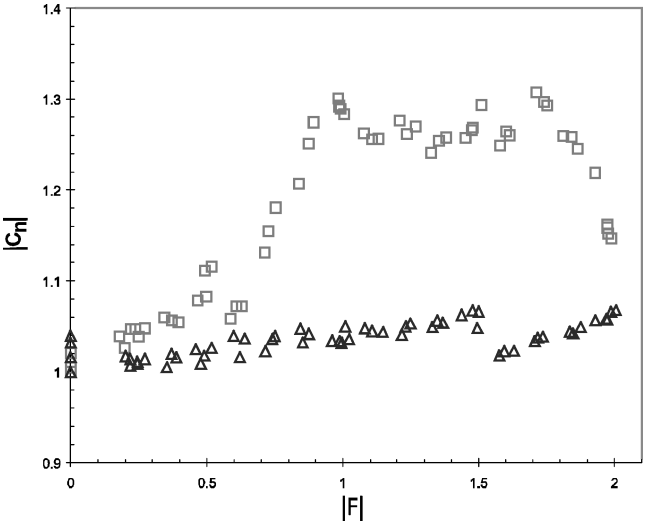

a) Normal force coefficient

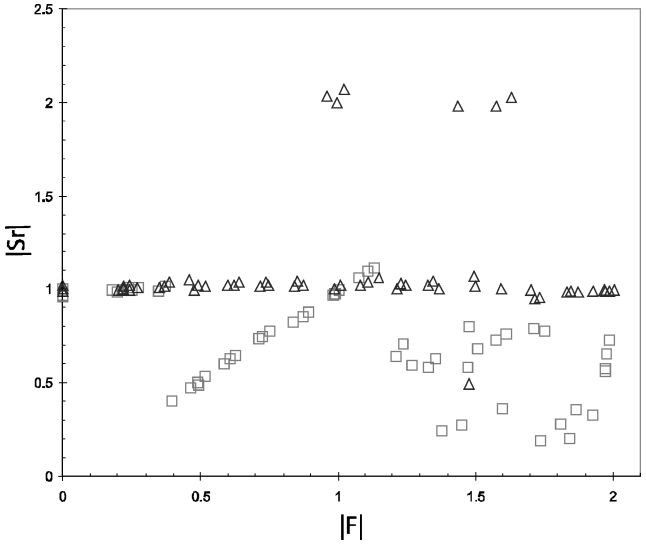

b) Strouhal number

Fig. 9 Variation with excitation frequency: angle of attack = 20 deg; □, leading-edge flap actuation and △, trailing-edge flap actuation.

In Figs. 9–11, namely, for the low-angle-of-attack regime, we observe that the shedding frequency is locked on the driving frequency and for a wider range of $|F|$. Apparently, a very small disturbance introduced at the leading edge is enough to force the wake vortices to shed at the driving frequency. This is clearly indicated by the data falling along a line inclined by 45 deg. Notice also that lock-on is effective when the disturbance is introduced at the leading edge, but practically ineffective if the disturbance is applied at the trailing edge.

There is an intimate relationship between lock-on and normal force increase that may be explained as follows. For fully separated flows, vorticity shed from the leading and trailing edges rolls into large-scale vortical structures that form a von Kármán street. Vortices contain activated motion and, therefore, their proximity to a solid surface induces lower pressure and, thus, more lift, but this is a periodic phenomenon. Normal force and lift vary in time, and it is in the average that the lift increases. The closer the driving frequency is to the natural shedding frequency, the more effective the lock-on phenomenon. This means that vortices form closer to the airfoil and, therefore, induce higher lift in the average. This explains why the normal force increases with the driving frequency until the latter reaches the natural frequency.

The fluid flow excitation at the 20-deg angle of attack (Fig. 9) shows a peculiar behavior. In the range of the reduced frequency from 0 to 1, as discussed earlier, the normal force coefficient increases almost linearly with the driving frequency, with a small peak located at the subharmonic of the natural shedding frequency, and reaches a maximum 30% increase in a much more pronounced peak at the harmonic. Normal force increase is accompanied by a frequency lock-on, starting at $|F| = 0.4$ and continuing until $|F| = 1.13$, as shown in Fig. 9b. The normalized normal force coefficient displays an increase of about 25% in the range of 1–1.75 of $|F|$, dropping sharply for values beyond. The Strouhal number after the lock-on region drops to a value of around 0.5, showing a radical change in the vortex shedding pattern. A similar behavior is observed for angles of attack of 15 and 10 deg as shown in Figs. 10 and 11. In fact, the linear dependence of the normal force on the driving frequency is now very well pronounced, and the lift increases are larger, reaching 70%, as shown in Fig. 10.

Figures 12 and 13 show the PSD for two cases, one for a 30-deg angle of attack and the other for a 25-deg angle of attack. For both cases, a frequency lock-on takes place but with different effects. In Fig. 12, it can be seen that excitation organizes the vortical structure, locking the vortex shedding to the actuation frequency. Magnitude levels are lower overall, which implies that the vortex structure is weaker than in the base flow. Figure 13 is even more interesting. Not only is the shedding locking on to this new value, but the vortical formation is completely destroyed as indicated by a broader energy spectrum over a wider range of scales. This is the opposite of the desired goal.

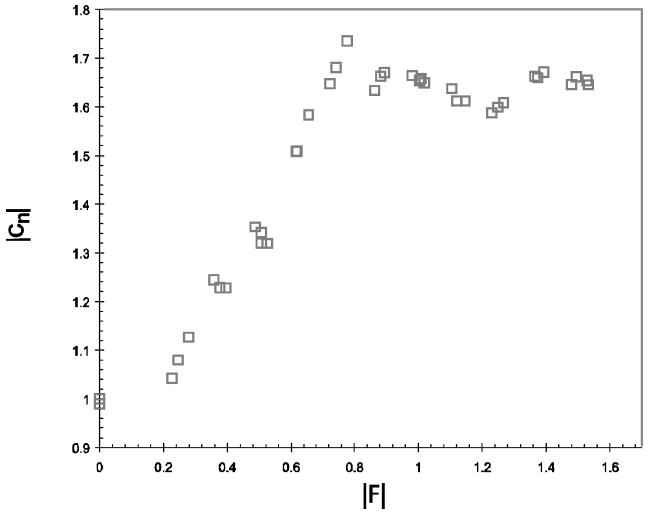

a) Normal force coefficient

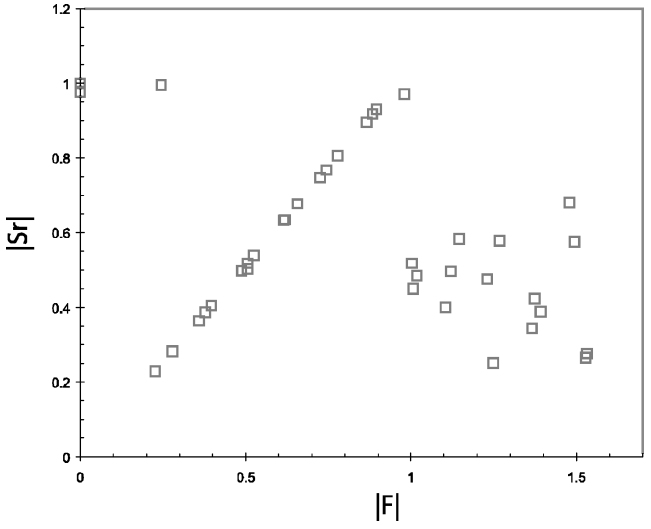

b) Strouhal number

Fig. 10 Variation with excitation frequency: angle of attack = 15 deg; □, leading-edge flap actuation.

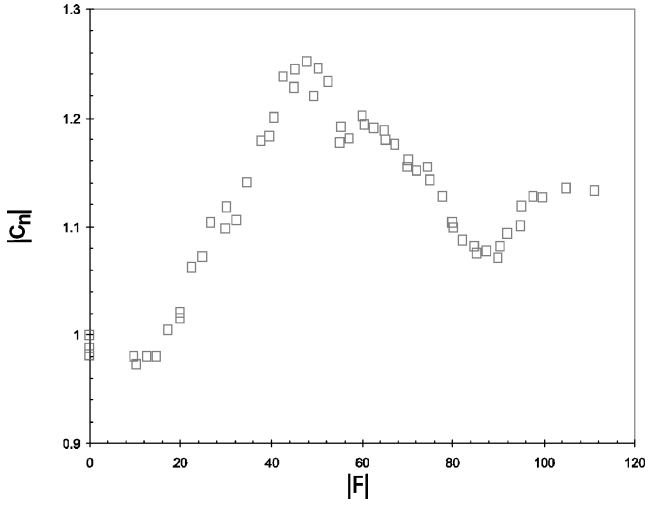

a) Normal force coefficient

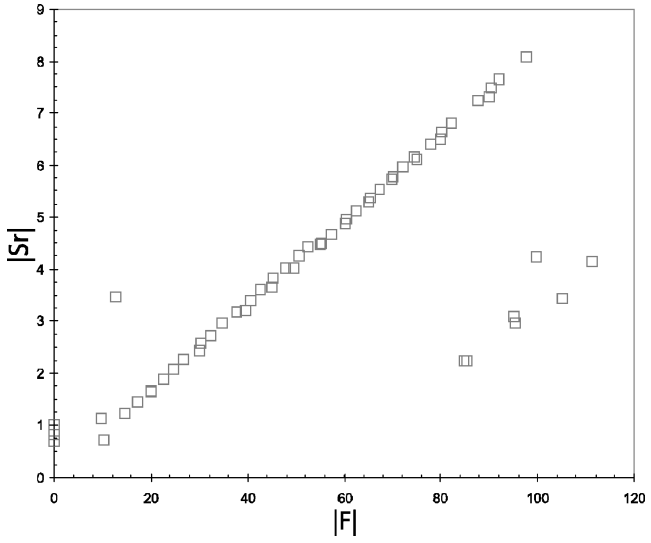

b) Strouhal number

Fig. 11 Variation with excitation frequency: angle of attack = 10 deg; □, leading-edge flap actuation.

The pressure coefficient distribution over the airfoil at $\alpha = 20$ deg is shown in Fig. 14. Figure 14 shows that both values of reduced frequency, $|F| = 1$ and 1.5, promote the same lift increment, but with a difference in the vortex structure on the suction side of the airfoil. The pressure distribution on the suction side for $|F| = 1.5$ is slightly higher for the first 50% of the chord and drops toward the trailing edge. The excitation at the natural shedding frequency behaves in the opposite way. The C_p increases slightly toward the trailing edge. This implies that a different mode of vortex formation is promoted. This effect must have an important implication on the moment coefficient of the airfoil. A change in excitation frequency can shift the position of the aerodynamic center while retaining the magnitude of lift.

The 15-deg angle of attack generates the maximum lift increase on the airfoil, resulting in a 73% lift increment for a reduced frequency of about 0.75, as shown in Fig. 10a. It is encouraging that lift increases linearly from the lowest reduced flap frequency tested to the most efficient one. This linearity may be useful if control of an aircraft is desired. After its highest value, the normal force coefficient settles at an average value of 1.63, showing some slight variations with flap frequency. The Strouhal number plot in Fig. 10b shows that the linear increase is accompanied with a perfect frequency lock-on to the excitation frequency. This lock-on phenomenon extends up to the frequency of natural vortex shedding. Beyond this value, the shedding frequency drops to an average of the subharmonic value.

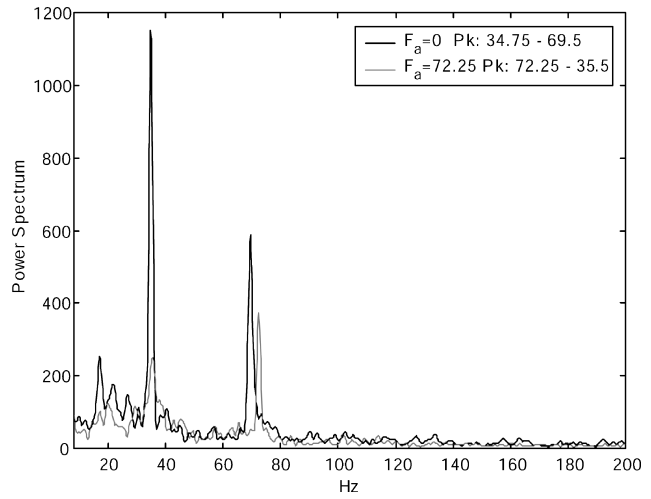

Fig. 12 PSD of pitot 3 at excitation $|F| = 2.06$, angle of attack = 30 deg, Pk indicates peaks.

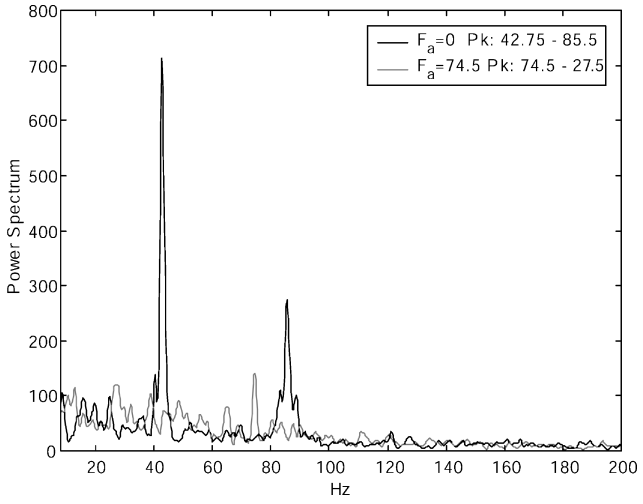

Fig. 13 PSD of pitot 3 at excitation $|F| = 1.75$, angle of attack = 25 deg; Pk indicates peaks.

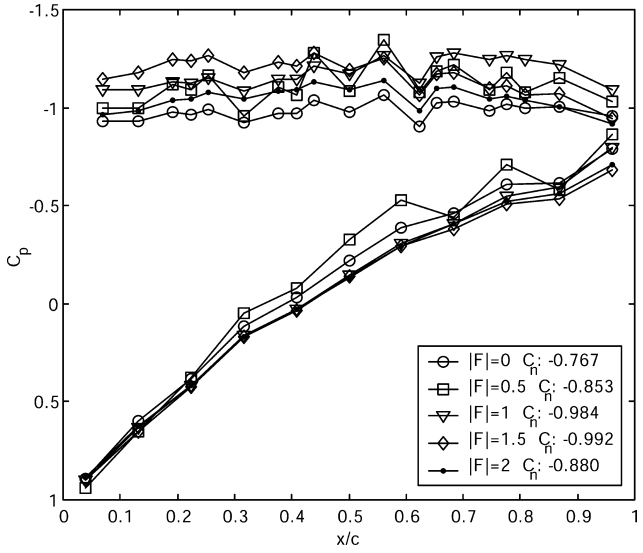

Fig. 14 Pressure coefficient distribution for controlled case: angle of attack = 20 deg, leading-edge excitation.

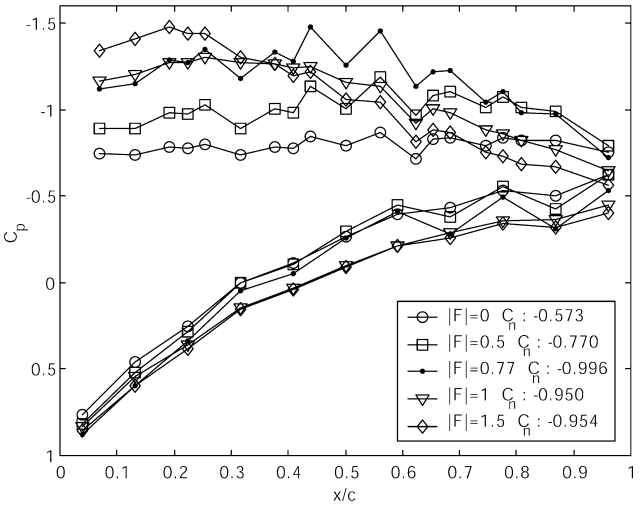

Fig. 15 Pressure coefficient distribution for controlled case: angle of attack = 15 deg, leading-edge excitation.

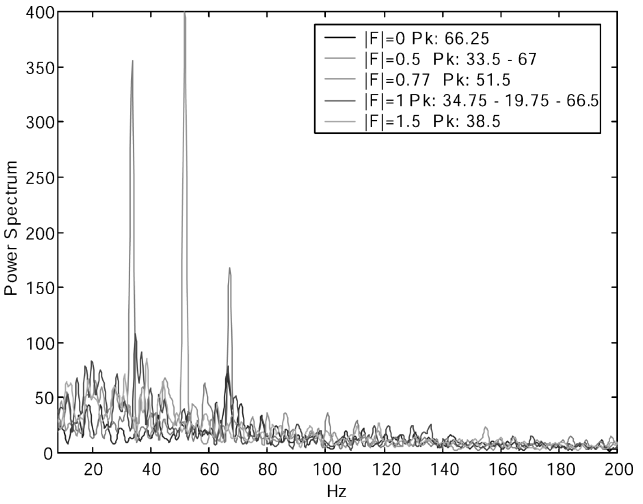

Fig. 16 PSD of pitot 3 for controlled case: angle of attack = 15 deg, leading-edge excitation.

Figure 15 displays pressure distributions over the airfoil for the 15-deg case. Reduced frequencies of 0.5 and 0.77 lead to lower suction-side pressure distributions, that is, increasing lift. Lower pressure values in the middle of the chord indicate that a vortex positioned in the middle of the airfoil gains strength with excitation. This implies that the flow tends to reattach close to the trailing edge. This can be seen by simple extrapolation of the measured values for both the suction and pressure side and verification that the Kutta condition is met. For actuation frequencies $|F| = 1$ and $|F| = 1.5$, the behavior found in the 20-deg case is also observed, namely, whereas for $|F| = 1$ there is a tendency for spreading the pressure distribution along the extent of the chord, for $|F| = 1.5$ a suction peak at about $x/c = 0.2$ develops. Both $|F| = 1$ and $|F| = 1.5$ induce a mild pressure side pressure increase.

For $\alpha = 15$ deg, we observe in the PSD plot in Fig. 16 that for the optimum frequency, a very coherent flow is achieved. A very-narrow-band spike implies an organized vortical structure on the suction side of the airfoil, and the magnitude indicates a strong enhanced vortex. The frequency at which the vortex is enhanced is not related to the natural shedding frequency. This observation is in agreement with the maximum increase of the normal force being found again for this frequency, a little lower than the natural frequency, as shown in Fig. 10a. Excited at the subharmonic of the natural frequency, the subharmonic and the natural shedding frequencies are visibly enforced. The higher excitation frequencies do not organize the flow as those discussed so far. The frequency spectrum for the latter has broader peaks and low magnitudes. This behavior is clearly displayed in the temporal variations of the normal force in Fig. 17, where we observe that when lift increases are obtained, the oscillation amplitude increases too.

For the smallest angle of attack tested, $\alpha = 10$ deg, a different behavior of the flow control over the circular-arc airfoil is observed as shown in Fig. 11a. As mentioned before, we could not detect a natural shedding frequency for this case. The calculated frequency should lie around 100–110 Hz. Following the recommendation of one of the reviewers, we carried out some flow visualizations. This was done in our water tunnel and with a model and speed that match the Reynolds number of the wind-tunnel tests. Flow visualization was carried out by time exposure of seed particles. These are neutrally buoyant spheres, about 10 μm in diameter. With exactly the same arrangement but with much shorter exposure, we obtained data that were later processed by our particle image velocemetry (PIV) software. The reader can find extensive descriptions of our system and its capabilities in Ref. 16. In Fig. 18a we show a visualization of the flow in the wake of a sharp-edged wing. In Fig. 18b, we show vorticity contours calculated in terms of the corresponding PIV data. Vortex shedding is clearly detected in both of the frames of Fig. 18. Our wake sensors may have not been placed in the appropriate position to pick up the corresponding fluctuation.

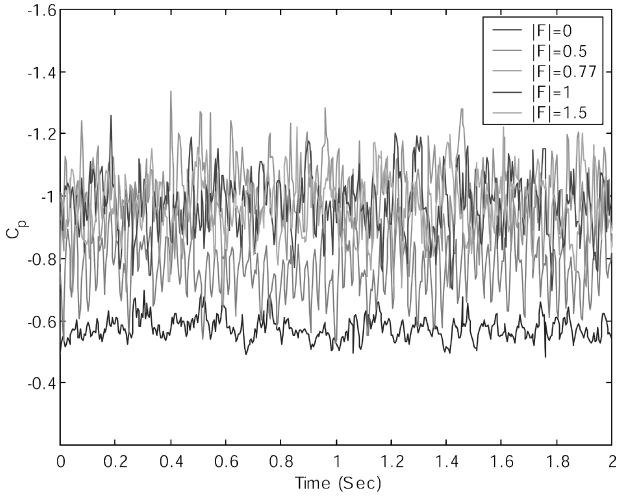

Fig. 17 Evolution of normal force coefficient for different actuation frequencies: angle of attack = 15 deg, leading-edge excitation.

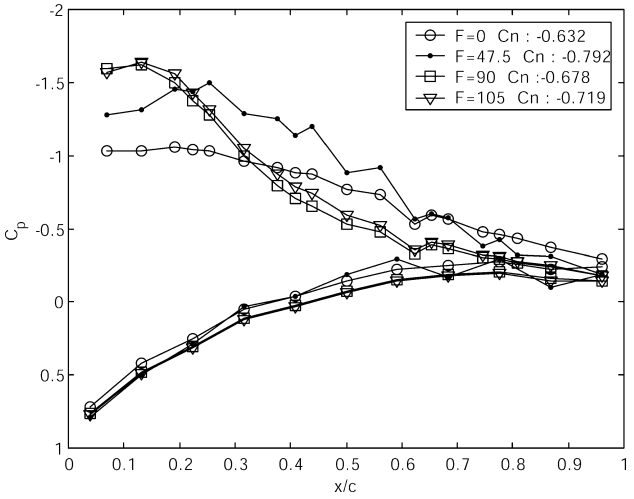

Fig. 19 Pressure coefficient distribution for controlled case: angle of attack = 10 deg, leading-edge excitation.

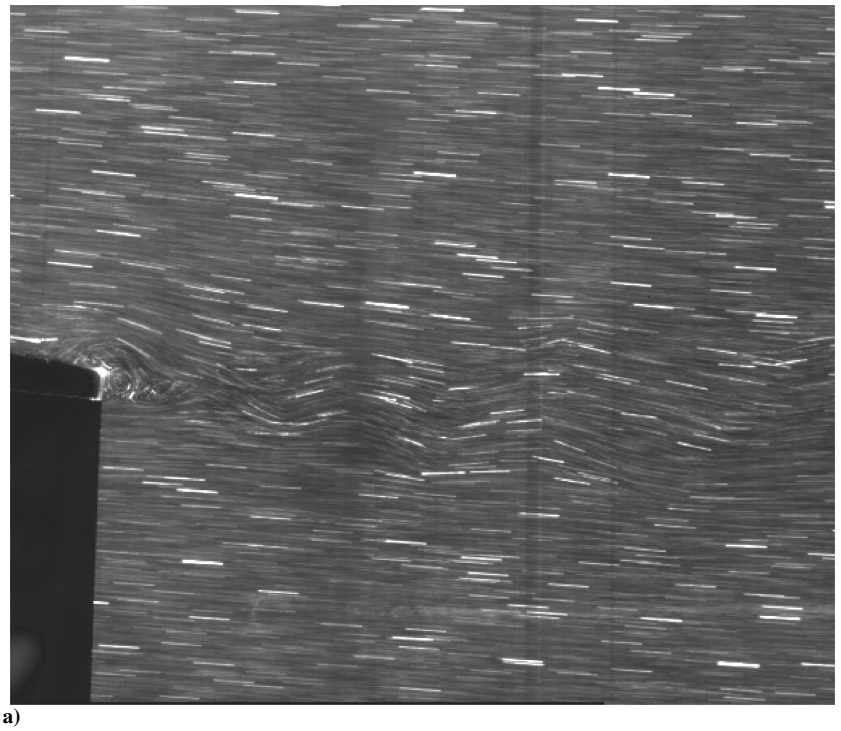

a)

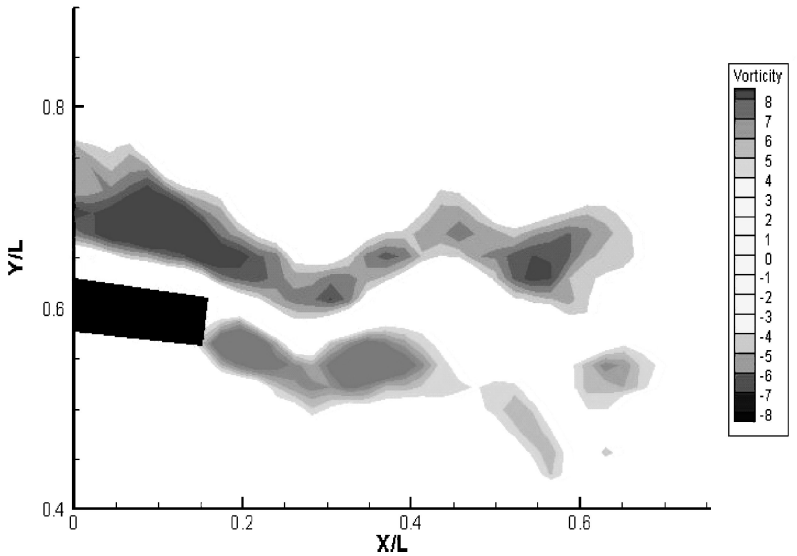

b)

Fig. 18 PIV data calculation: a) particle flow visualization and b) instantaneous vorticity contours; length scale L equals chord, wing is at $\alpha = 10$ deg, and wing's trailing edge is at top right-hand corner of shaded shape.

As control is applied in the case of $\alpha = 10$ deg, the effect on the normalized normal force coefficient is similar to that of the 15-deg case (Fig. 11a). The difference is that $|C_n|$ increases with frequency until a maximum of 25% but then steadily decreases to a value of 7%. Then, a new increase of the normal force occurs and settles at 15%. This strange behavior could be explained from the Strouhal number plot. It is clear that a perfect frequency lock-on is enforced on the shedding frequency and that frequency lock-on is extended until a maximum frequency of around 95–97 Hz is reached. This is close to the estimated shedding frequency. This is not a coincidence. The changes in the trends of $|C_n|$, that is, increasing or decreasing values, occur at the subharmonic of the natural frequency. If we assume that 95–97 Hz is the natural shedding frequency, then the most efficient point occurs at the subharmonic frequency of shedding. Similarly, the second increase of lift settles down to a maximum at around the uncontrolled predicted shedding frequency.

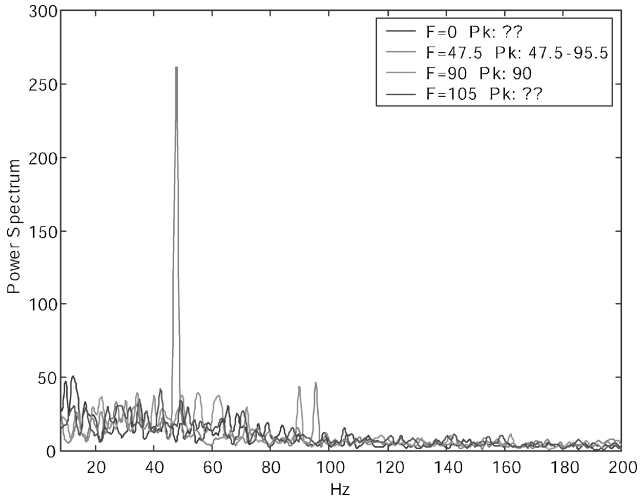

Fig. 20 PSD of pitot 3 for controlled case: angle of attack = 10 deg, leading-edge excitation.

Pressure distributions and power spectra are shown in Figs. 19 and 20, respectively. Normal force coefficient increments are not as impressive as that for the 15-deg case, but overall lift is augmented. Figure 20 shows the effects of excitation in this particular case. Note that the only frequency that really triggers the shedding phenomenon is that of the estimated subharmonic flap frequency. In other words, no peak can be found for no excitation, but the small disturbance introduced by our microflap is enough to induce a well-organized structure over the suction side of the airfoil. The lock-on frequency is evident, but so is a component at twice that frequency, namely, the estimated natural vortex shedding is apparent. For the other excitation values, the flow structure is not enhanced, as can be seen from the broad frequency spectrum.

The pressure distributions shown in Fig. 19 are also unexpected and unusual. Whereas the highest excitation frequencies seem to promote reattachment of the flow, the optimum reduced frequency creates a vortex in the average sense over the suction surface, which leads to further increases of the suction force. The flow is also reattached in the average sense, but at a point further downstream.

The classical thinking that lift will increase only by forcing the flow to reattach is not necessarily true. If periodic excitation is applied, it is possible to capture a large vortex in the average and, therefore, provide even more lift than in the fully attached flow case.

All of our normal force coefficient results were calculated based on the assumption that the surface of the airfoil is flat, that is, we assumed that locally the force elements are normal to the chord. A more careful calculation that takes into account the slight curvature of the wing indicates somewhat different values. For example, for $\alpha = 10$ deg, we calculated C_L of 0.699 and 0.715 with a flat and a curved surface, respectively. The same calculations for the controlled case yielded 0.881 and 0.886, respectively.

The only other data on sharp-edged airfoils we could compare our results with are those of Cahil et al.[15] These authors present lift, drag, and moments for a large number of flap configurations but pressure data for only a few cases, none of which corresponds to ours. It was, therefore, not possible to compare pressure distributions with those of Ref. 15. On the other hand, Cahil et al. present detailed lift-vs-angle-of-attack graphs. We do not have data for a sequence of angles

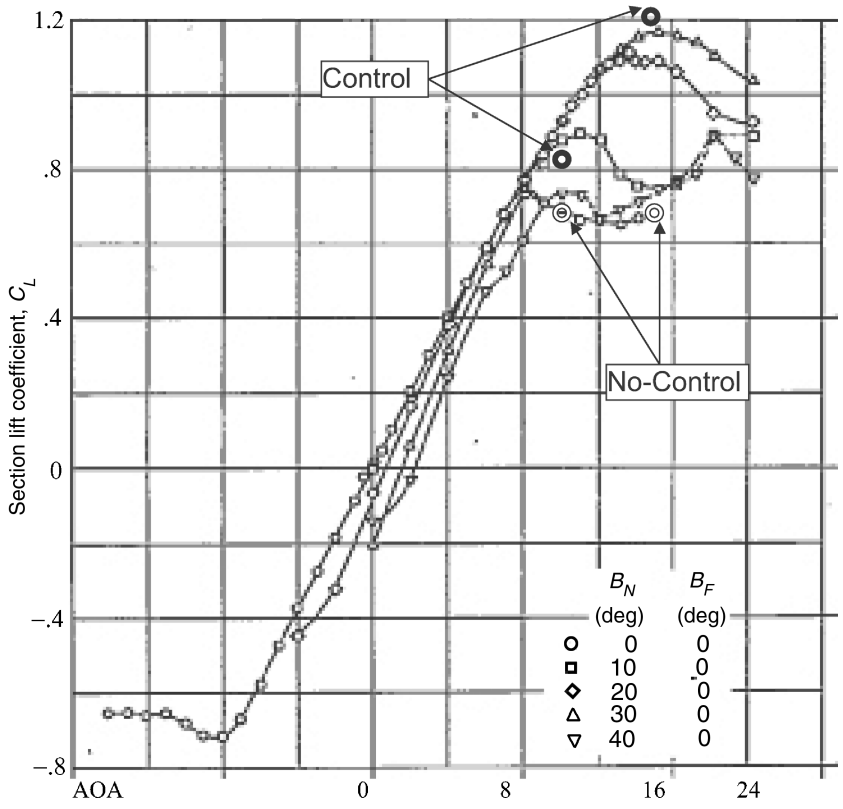

Fig. 21 Lift curves from Ref. 15, present data added for two angles of attack for the control and no-control cases.

of attack, but we were able to facilitate comparison by placing on their graph our data for $\alpha = 10$ and 15 deg for the control and no-control case. This is shown in Fig. 21. It appears that our data for the no-control case are in full agreement with the results in Ref. 15 for no-flap deployment. Cahil et al. tested the effectiveness of a large leading-edge flap, the angle of which is listed in their figure and marked in their nomenclature with the symbol δ. We could, therefore, compare the effectiveness of a large mechanical flap to that of our flow control device. It is most encouraging that flow control achieves a little more increase of the lift than the deployment of a large flap.

Conclusions

We demonstrated experimentally that separated flow over sharp-edged airfoils could be managed by the introduction of small periodic disturbances at the leading or trailing edge. Unlike most other studies, we control here not the location of separation, but separated flow itself. In other words, we accept that massive separation exists, and we try to modify it to our benefit. Our results indicate that lift could be increased on average by as much as 70%.

We followed techniques established by researchers in flow-induced vibrations. We vary the driving frequency by small increments and for a wide range of frequencies. This was possible because our actuation mechanism is equally effective at all of the frequencies tested. We demonstrated that vortex shedding can lock on the driving frequency for a wide range of frequencies. We proved that the flow control phenomenon under consideration is robust. The shedding events lock on the externally introduced disturbance for a wide range of actuation frequencies. This means that the control mechanism could be relied on to achieve increases of lift without the need to match the natural shedding frequency or its subharmonic.

We found that the mechanism employed is more effective for angles of attack up to 20 deg. Very small increases in lift were found for angles of attack equal to 25, 30, and 40 deg. Note that even at an angle of attack of 10 deg, for which no coherent oscillation in the wake was found with our instrumentation, actuation can reduce the extent of the separated region as detected by the suction side pressure distribution, which resembles more closely the distribution corresponding to attached flow. Driven at higher frequencies, there is evidence that a vortex is captured in the mean above the airfoil because the pressure distribution indicates a wide area of very low pressure.

Acknowledgments

Work on this paper was initiated with the encouragement of J. Z. Wu. Since then, the U.S. Air Force Office of Scientific Research (AFOSR) provided support for this effort under Grant AFOSR F49620-00-1-0335, Steven Walker, Monitor.

References

[1]Hsiao, F.-B., Liu, C.-F., and Shyu, J.-Y., "Control of Wall-Separated Flow by Internal Acoustic Excitation," *AIAA Journal*, Vol. 28, No. 8, 1990, pp. 1440–1446.

[2]Hsiao, F.-B., Shyu, R.-N., and Chang, R. C., "High Angle-of-Attack Airfoil Performance Improvement by Internal Acoustic Excitation," *AIAA Journal*, Vol. 32, No. 3, 1994, pp. 655–657.

[3]Hsiao, F.-B., Wang, T.-Z., and Zohar, Y., "Flow Separation Control of a 2-D Airfoil by a Leading-Edge Oscillating Flap," Pacific International Conf. of Aerospace Science Technology, Dec. 1993.

[4]Chang, R. C., Hsiao, F.-B., and Shyu, R.-N., "Forcing Level Effects of Internal Acoustic Excitation on the Improvement of Airfoil Performance," *Journal of Aircraft*, Vol. 29, No. 5, 1992, pp. 823–829.

[5]Zhou, M. D., Fernholz, H. H., Ma, H. Y., Wu, J. Z., and Wu, J. M., "Vortex Capture by a Two-Dimensional Airfoil with a Small Oscillating Leading-Edge Flap," AIAA Paper 93-3266, July 1993.

[6]Fiedler, H. E., "Control of Free Turbulent Shear Flows," *Flow Control: Fundamentals and Practices*, edited by M. Gad-el-Hak, A. Pollard, and J. P. Bonnet, Springer Lecture Notes in Physics, New Series Monographs, M53, Springer-Verlag, Berlin, 1998, pp. 335–429.

[7]Wu, J. Z., Lu, X. Y., Denny, A. G., Fan, M., and Wu, J. M., "Post-Stall Flow Control on an Airfoil by Local Unsteady Forcing," *Journal of Fluid Mechanics*, Vol. 371, 1998, pp. 21–58.

[8]Wu, J. Z., Vakili, A. D., and Wu, J. M., "Review of the Physics of Enhancing Vortex Lift by Unsteady Excitation," *Progress in Aerospace Sciences*, Vol. 28, 1991, pp. 73–131.

[9]Seifert, A., and Pack, L. G., "Oscillatory Control of Separation at High Reynolds Number," *AIAA Journal*, Vol. 37, No. 9, 1999, pp. 1062–1071.

[10]Seifert, A., and Pack, L. G., "Oscillatory Control of Separation at High Reynolds Numbers," AIAA Paper 98-0214, Jan. 1998.

[11]Roos, F. W., and Kegelman, J. T., "Control of Coherent Structures in Reattaching Laminar and Turbulent Shear Layers," *AIAA Journal*, Vol. 24, No. 12, 1986, p. 1956.

[12]Roos, F. W., and Kegelman, J. T., "Influence of Excitation on Coherent Structures in Reattaching Turbulent Shear Layers," AIAA Paper 86-0112, Jan. 1986.

[13]Roos, F. W., and Kegelman, J. T., "Structure and Control of Flow over a Backward-Facing Step," American Society of Mechanical Engineers, ASME 1987 Applied Mechanics, Bioengineering, and Fluid Mechanics Conf., June 1987.

[14]Roshko, A., "On the Drag and Shedding Frequency of Two-Dimensional Bluff Bodies," NACA TN 3169, July 1954.

[15]Cahil, F., Underwood, W. J., Nuber, R. J., and Cheesman G. A., "Aerodynamics Forces on Symmetrical Circular-Arc Airfoils with Plain Leading-Edge and Plain Trailing-Edge Flaps," NACA Rept. 1146, 1953.

[16]Abiven, C., and Vlachos, P. P., "Super Spatio-Temporal Resolution, Digital PIV System for Multi-Phase Flows with Phase Differentiation and Simultaneous Shape and Size Quantification," American Society of Mechanical Engineers, Int. Mech. Eng. Congress, JMECE-2002-33170, Nov. 2002.

H. Reed
Associate Editor